# Trends of Neutron Skins and Radii of Mirror Nuclei from First Principles

S. J. Novario,[1] D. Lonardoni,[1,*] S. Gandolfi,[1] and G. Hagen[2,3]
[1]Theoretical Division, Los Alamos National Laboratory, Los Alamos, New Mexico 87545, USA
[2]Physics Division, Oak Ridge National Laboratory, Oak Ridge, Tennessee 37831, USA
[3]Department of Physics and Astronomy, University of Tennessee, Knoxville, Tennessee 37996, USA

(Received 2 December 2021; revised 4 April 2022; accepted 13 December 2022; published 19 January 2023)

The neutron skin of atomic nuclei impacts the structure of neutron-rich nuclei, the equation of state of nucleonic matter, and the size of neutron stars. Here we predict the neutron skin of selected light- and medium-mass nuclei using coupled-cluster theory and the auxiliary field diffusion Monte Carlo method with two- and three-nucleon forces from chiral effective field theory. We find a linear correlation between the neutron skin and the isospin asymmetry in agreement with the liquid-drop model and compare with data. We also extract the linear relationship that describes the difference between neutron and proton radii of mirror nuclei and quantify the effect of charge symmetry breaking terms in the nuclear Hamiltonian. Our results for the mirror-difference charge radii and binding energies per nucleon agree with existing data.

DOI: 10.1103/PhysRevLett.130.032501

*Introduction.*—The size of neutron stars and the distributions of excess neutrons in medium-mass and heavy nuclei can be linked to the microscopic forces between the constituent nucleons that build up the atomic nucleus and the equation of state of nucleonic matter [1–4]. With recent advancements in both observational astrophysics and experimental nuclear physics, investigating this link and constraining nuclear models are now becoming possible. The advent of multimessenger astronomy, established with the simultaneous observation of a binary neutron star merger by the LIGO gravitational-wave observatory [5,6] and gamma-ray astronomy, has opened up the possibility of examining the structure of neutron stars in new detail [7]. Furthermore, experiments have been designed to determine the neutron distributions in nuclei, including the recent extractions of the neutron skin from measurements of the parity-violating asymmetry in $^{208}$Pb [8,9] and $^{48}$Ca [10].

The neutron skin thickness $\Delta R_{\mathrm{np}}$ is defined as the difference between the root-mean-squared (rms) point radii of the neutron and proton density distributions. Collectively, the neutron skin results from a balance between the inward pressure of the surface tension on excess neutrons on the edge of the nucleus and outward degeneracy pressure from excess neutrons within the core of the nucleus. The same balance is reached in neutron stars with the inward pressure of gravity. The relationship between this pressure and the neutron density is quantified in the slope of the symmetry energy at saturation density $L$. Therefore, this bulk property of neutron stars should be related to the neutron skin of nuclei [1,2,11–15].

Recent high-precision measurements of charge radii in isotope chains of potassium [16], calcium [17,18], nickel [19], copper [20,21], and silver [22] have revealed that they carry information about changes in shell structure, deformation, and pairing effects. Charge radii can be easily probed with the well-known electromagnetic interaction [23,24]. Conversely, measuring the neutron (weak-charge) radius is more difficult, but can be accomplished using either strong or electroweak probes, each with their own shortcomings. Hadronic probes suffer from model-dependent uncertainties [25], and electroweak probes, like those used in PREX [8,9] and CREX [10], measure the parity-violating asymmetry at one momentum transfer and extract the neutron skin using different models. As argued in Ref. [26] a clean comparison between theory and experiment would be to compute this quantity instead of the neutron skin. The issue with model dependencies in extracting the neutron skin can be overcome in some cases [8,9], but precision measurements of the neutron radius for short-lived isotopes remain elusive.

In this Letter, we study trends in the neutron skin thickness of light- and medium-mass mirror nuclei with mass number $6 \leq A \leq 56$ (shown in Fig. 1) by computing the proton and neutron radii using the *ab initio* coupled cluster (CC) [27–33] and auxiliary field diffusion Monte Carlo (AFDMC) methods [34–36], each with different nuclear interactions derived from chiral effective field theory (described below). These methods are validated by comparing our computed mirror-difference charge radii and binding energies per nucleon with available data (shown in Fig. 4). We then confirm the linear relation between neutron skin thickness and isospin asymmetry from the liquid-drop model (LDM) and compare this relation with the available experimental data. Additionally, we also confirm a similar linear relation with the difference between the neutron and proton radii of mirror partners and connect this relation to the

 

LDM. Finally, we estimate the contribution of isospin-symmetry-breaking terms in the interaction by calculating ground-state energies and radii with and without the Coulomb interaction.

*Methods.*—We describe nuclei as a collection of $A$ pointlike nucleons of average mass $m$ interacting according to the nonrelativistic intrinsic Hamiltonian

$$H = -\frac{\hbar^2}{2mA}\sum_{i<j}(\nabla_i - \nabla_j)^2 + \sum_{i<j}V_{ij} + \sum_{i<j<k}V_{ijk}. \quad (1)$$

Here, $V_{ij}$ and $V_{ijk}$ are the nucleon-nucleon and three-nucleon potentials, respectively, the former of which also includes the Coulomb force. Interactions used in this Letter are derived from chiral effective field theory (EFT) [37–44]. As this Letter focuses on bulk properties of nuclei, we choose a subset of chiral interactions that have been shown to accurately reproduce these quantities. The first, $\mathrm{N^2LO_{sat}}$ [45], was optimized to few-body observables as well as radii and ground-state energies of selected carbon and oxygen isotopes. The second and third, $\Delta\mathrm{N^2LO_{GO}}(394)$ and $\Delta\mathrm{N^2LO_{GO}}(450)$ [46–48], include explicit $\Delta$ isobars and were optimized to few-body observables and properties of nucleonic matter, and use momentum cutoff of $\Lambda = 394$ MeV/$c$ and $\Lambda = 450$ MeV/$c$, respectively.

After establishing the nuclear interactions, we perform a Hartree-Fock diagonalization from a spherical harmonic-oscillator basis and then construct a prolate, axially-deformed product state built from natural orbitals [49,50]. We then normal-order the Hamiltonian with respect to the reference state, denoted by $|\Phi_0\rangle$, and retain one- and two-body terms [51,52]. Next, we use the coupled-cluster method in the singles-and-doubles (CCSD) approximation to construct the similarity-transformed Hamiltonian, $\bar{H}_N = e^{-\hat{T}}H_N e^{\hat{T}}$, which decouples the reference state from excitations around it. In the CCSD approximation the cluster operator $\hat{T}$ is truncated at the $2p$–$2h$ excitation level. Because $\hat{T}$ is asymmetric, $\bar{H}_N$ is non-Hermitian, and the left ground state must be decoupled separately using $\langle\Phi_0|(1+\hat{\Lambda})$, where $\hat{\Lambda}$ is a de-excitation analog to $\hat{T}$ [32,33] and is also truncated at the $2p$–$2h$ level. In this Letter we are interested in computing the ground-state expectation value of the squared intrinsic point-nucleon radius operator, $\hat{r}^2$. In CC theory this operator is similarity transformed according to $\bar{r}^2 \equiv e^{-\hat{T}}\hat{r}^2 e^{\hat{T}}$, and applied between the left and right CC ground states, i.e., $\langle\hat{r}^2\rangle \equiv \langle\Phi_0|(1+\hat{\Lambda})\bar{r}^2|\Phi_0\rangle$.

We also perform AFDMC calculations of the point-proton and neutron radii (see Ref. [36] for more details) using a local chiral nucleon-nucleon and three-nucleon interaction at next-to-next-to-leading order, $\mathrm{N^2LO_{E\mathbb{1}}}$ [36,53–55]. This interaction has been used to study the ground-state properties of nuclei up to $^{16}$O [36,55–63], few neutron systems [64–66], and neutron star matter [54,55,67–76]. Additionally, among other *ab initio* methods (see Ref. [77] for a recent review), both CC and AFDMC have been used to accurately calculate nuclear radii, e.g., [16,19] and [58,78], respectively.

*Results.*—Our results for the neutron skin thickness of selected nuclei with $6 \le A \le 56$ are shown in Fig. 1. These data are plotted against the isospin asymmetry, $I = (N-Z)/A$, with $N$ and $Z$ being the number of neutrons and protons, respectively, and a linear relationship is extracted. This relationship was first derived from the LDM in Refs. [79–82] and demonstrated with mean-field methods in Ref. [83]. We fit the data using linear regression which is shown in Fig. 1 as shaded gray bands at $1\sigma$, $2\sigma$, and $3\sigma$ confidence levels. The fit uncertainties increase away from $I = 0$, and the quoted uncertainties are taken from the maximum value from within the data.

There are several distinct sources of uncertainties in the CC calculations. First, the error associated with the finite size of the employed model space is estimated by taking the difference between the squared radii calculated in the model spaces of $N_{\max} = 10$, 12, respectively, where $N_{\max} = (2n+l)_{\max}$ indicates the maximum harmonic oscillator energy level. We also note that in this Letter we utilize a basis with an oscillator energy of $\hbar\omega = 16$ MeV, which is suitable for all calculated nuclei. The additional uncertainty associated with this choice is estimated to be 1% [50,84]. Second, the uncertainty associated with truncating the CC excitation operator at the $2p$–$2h$ level amounts to another 1% uncertainty [50,84,85]. Finally, the error from breaking rotational symmetry is estimated to be less than 1% on computed radii (see Ref. [86] for details). Uncertainties on

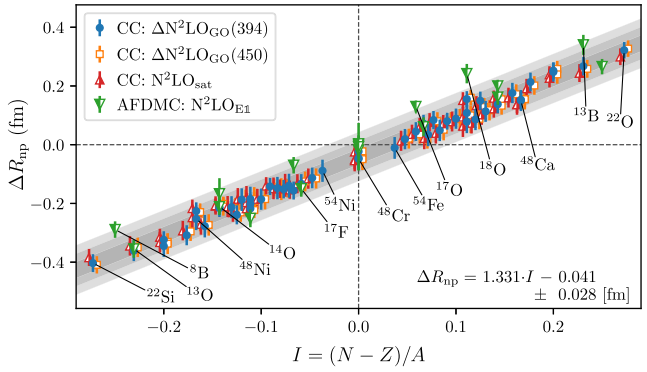


FIG. 1. Neutron skin thickness plotted against the isospin asymmetry from *ab initio* calculations. Coupled-cluster results of nuclei with $14 \le A \le 56$ using the $\Delta\mathrm{N^2LO_{GO}}(394)$, $\Delta\mathrm{N^2LO_{GO}}(450)$, and $\mathrm{N^2LO_{sat}}(450)$ interactions are shown as solid blue circles, empty orange squares, and right-filled red triangles, respectively. Left-filled green triangles represent auxiliary field diffusion Monte Carlo results for $6 \le A \le 18$ using the $\mathrm{N^2LO}_{E\mathbb{1}}$ local chiral interaction. The linear regression is printed in the bottom right with $1\sigma$ uncertainty, and the $1\sigma$, $2\sigma$, and $3\sigma$ confidence levels are shown as gray bands. Select nuclei are labeled.

AFDMC results are statistical, and are reported in this Letter at the $1\sigma$ confidence level. Errors on radii also include an extrapolation uncertainty from mix estimates, and those on binding energies from unconstrained evolution (see Ref. [36] for more details).

There are two main factors concerning the $A$ dependence of the linear relation in Fig. 1. First, it is expected that the collective behavior which gives rise to the linear dependence on the isospin asymmetry will be overshadowed by few-body effects for lighter nuclei. We note that among the five light nuclei computed with both methods, four neutron skin results were compatible. Second, there is an $A$ dependence that accounts for the Coulomb repulsion of the protons and can be derived from the LDM [79,82]. The first-order approximation to this effect is $\Delta R_{\rm np}^{\rm Coul} \approx -ZA^{-1/3} \times (r_0 c_1 / 8Q^*)$, where $r_0$ is the nuclear radius constant, $c_1$ is the Coulomb energy coefficient, and $Q^*$ is the effective surface stiffness coefficient (see Supplemental Material [87] for details). Using values from Ref. [79], this contribution can be approximated as $\Delta R_{\rm np}^{\rm Coul} \approx -ZA^{-1/3} \times 0.0033$ fm.

To test the validity of our linear relationship between neutron skin thickness and the isospin asymmetry, we plot the Coulomb-subtracted neutron skin thickness ($\Delta R_{\rm np}^{*} = \Delta R_{\rm np} - \Delta R_{\rm np}^{\rm Coul}$) in Fig. 2 for experimental data of neutron-rich nuclei along with the linear regression of our data at the $1\sigma$ confidence level, which is shown by two dashed black lines. Most of the experimental data are extracted from x-ray spectroscopy following antiprotonic annihilation [90,91]. These data are used to fit a linear relationship which is shown as a green band and denoted as $\Delta R_{\rm np}^{*<}$. Additional data from proton scattering are also included [92,93] and separately fit, which is shown as a blue band and denoted as $\Delta R_{\rm np}^{*>}$. Also shown are the results from CREX [10], PREX-I [8], and PREX-II [9], which extract the neutron radius of $^{48}$Ca and $^{208}$Pb from parity-violating electron scattering, respectively.

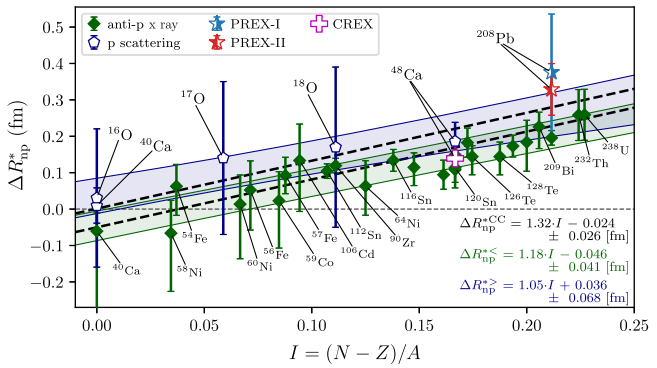


FIG. 2. Coulomb-subtracted neutron skin thickness ($\Delta R_{\rm np}^{*} = \Delta R_{\rm np} + ZA^{-1/3} \times 0.0033$ fm) plotted against the isospin asymmetry from available experimental data. Solid green diamonds are the results extracted from antiprotonic x-ray data [90,91] and open blue pentagons are from proton scattering [92,93]. These data are accompanied by linear fits shown as green and blue bands, respectively, and both relations are printed in the bottom right ($\Delta R_{\rm np}^{*<}$ and $\Delta R_{\rm np}^{*>}$). The right-filled blue star and the left-filled red star are the values for $^{208}$Pb from PREX-I [8] and PREX-II [9], respectively. The open cross is the value for $^{48}$Ca from CREX [10]. These experimental data are compared with our *ab initio* results, shown as dashed black lines from the $1\sigma$ limits of a linear regression.

Our linear fit overlaps significantly with both the antiprotonic x-ray and proton-scattering data but has a larger slope. In the LDM, this slope is related to the ratio of the symmetry-energy coefficient $J$ and the effective stiffness coefficient ($\approx 3r_0 J/2Q^*$). Using the slope from our results, we obtain a ratio of $J/Q \approx 1.59$ which is larger than those obtained with many Skyrme forces [94] but consistent with the values from Ref. [79]. Using our linear relationship to predict the neutron skin of $^{208}$Pb, we obtain $\Delta R_{\rm np}(^{208}{\rm Pb}) = 0.210 \pm 0.026$ fm, which is consistent with the recent *ab initio* prediction in Ref. [95].

The bulk properties that give rise to the neutron skin can also be utilized to establish a relationship between the point-proton radius of a nucleus, $R_{\rm p}$ and the point-neutron radius of its mirror partner, $R_{\rm n}^{\rm mirror}$. In the limit of conserved isospin symmetry, these two quantities should be exactly equal so that $\Delta R_{\rm np}^{\rm mirror} = R_{\rm n}^{\rm mirror} - R_{\rm p} = 0$. The first-order correction to this limit from the LDM [79,82] is the same as for the neutron skin thickness, $\Delta R_{\rm np}^{\rm Coul}$. However, in this case the Coulomb-subtracted difference, $\Delta R_{\rm np}^{*\rm mirror}$ should be proportional to $I \times A$ such that $\Delta R_{\rm np}^{*\rm mirror}/A \approx I \times (r_0 c_1 / K)$, where $K$ is the compressibility coefficient (see Supplemental Material [87] for details).

To test this relationship, we plot the Coulomb-subtracted difference, $\Delta R_{\rm np}^{*\rm mirror}$, against the isospin asymmetry in Fig. 3. The nonzero intercept results from higher-order

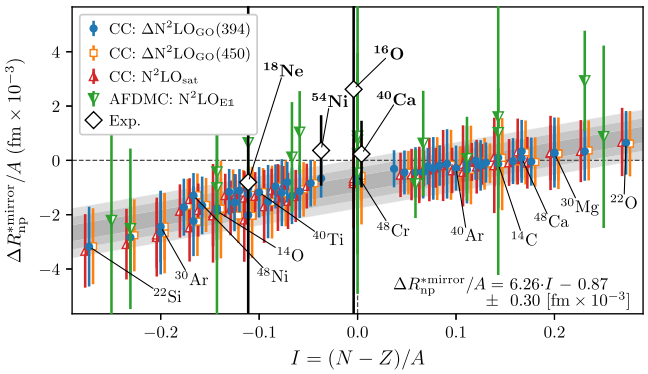


FIG. 3. Coulomb-subtracted mirror neutron skin thickness $\Delta R_{\rm np}^{*\rm mirror}/A = (\Delta R_{\rm np}^{\rm mirror} + ZA^{-1/3} \times 0.0033$ fm$)/A$ plotted against the isospin asymmetry. The data markers are the same as those in Fig. 1. The experimental data for $^{16}$O ($^{18}$Ne), $^{40}$Ca, and $^{54}$Ni are extracted from Refs. [24,90–92,96]. The linear regression is printed in the bottom right with $1\sigma$ uncertainty, and the $1\sigma$, $2\sigma$, and $3\sigma$ confidence levels are shown as gray bands. Selected nuclei are labeled.

Coulomb corrections and shell effects. The slope is related to the compressibility coefficient, which can be extracted as $K \approx 138$ MeV, a smaller value compared with the range from the interactions used in this Letter (150 MeV $\leq K \leq$ 250 MeV [12,48,75]). In addition to our results, we also show experimental data for $^{16}$O, $^{18}$Ne, $^{40}$Ca, and $^{54}$Ni. The proton radii are extracted from Refs. [24] and [96] for $^{54}$Ni. The neutron radii are then extracted from the neutron skins in Refs. [90–92] and charge radii in Ref. [24]. This relationship in Fig. 3 can be employed to determine the elusive neutron radius of a nucleus by more easily measuring the proton radius of its mirror nucleus. While some of the proton-rich nuclei in these calculations are near the drip-line, the Coulomb barrier ensures that their ground states are weakly coupled to nearby proton-continuum states. Therefore, these nuclei can be accurately described by bound-state methods including CC [97–101].

The near equivalence between $R_{\rm n}^{\rm mirror}$ and $R_{\rm p}$, shown in Fig. 3, suggests a correspondence between the neutron skin and the mirror-difference charge radii, $\Delta R_{\rm ch}^{\rm mirror}({}^{A}_{Z}X_N) = [R_{\rm ch}({}^{A}_{N}Y_Z) - R_{\rm ch}({}^{A}_{Z}X_N)]$. We compute the mirror-difference charge radii for selected nuclei and compare with available experimental data, shown in Fig. 4. The charge radius is computed using the formula $R_{\rm ch}^2 = R_{\rm p}^2 + \langle r_{\rm p}^2\rangle + (N/Z)\langle r_{\rm n}^2\rangle + \langle r_{\rm DF}^2\rangle + \langle r_{\rm SO}^2\rangle$ where the spin-orbit correction, $\langle r_{\rm SO}^2\rangle$, is calculated with the CC method [12], and $\langle r_{\rm p}^2\rangle = 0.709$ fm$^2$, $\langle r_{\rm n}^2\rangle = -0.106$ fm$^2$, and $\langle r_{\rm DF}^2\rangle = 3/(4m^2) = 0.033$ fm$^2$ are the charge radius squared of the proton [102,103], the neutron [104], and the Darwin-Foldy term, respectively. Our results agree well with the sparse data, most of which were taken from Ref. [24] except for those of $^{36}$Ca [18] and $^{54}$Ni [96]. Because $\Delta R_{\rm ch}^{\rm mirror}$ is an analog of the neutron skin, it also has a linear relation to the isospin asymmetry. Also shown in Fig. 4 is the comparison of our results with data from Ref. [88] of mirror-difference binding energies per nucleon $\{\Delta({\rm BE}/A)({}^{A}_{Z}X_N) = [{\rm BE}({}^{A}_{Z}X_N) - {\rm BE}({}^{A}_{N}Y_Z)]/A\}$. This quantity exhibits a linear relationship with the Coulomb asymmetry, $I_{\rm C} = [I(A-1)]/A^{1/3}$, which stems from the only mirror-asymmetric term in the LDM. The absolute binding energies per nucleon and charge radii are also compared to experimental data in the Supplemental Material [87].

Finally, we also study the extent of the isospin-symmetry-breaking terms in the nuclear interaction by computing ground-state energies and radii of select mirror nuclei using CC theory with and without the Coulomb term. We show these results for $A = 42 - 48$ using $\Delta{\rm N^2LO_{GO}}(394)$ in Table I, for the neutron skin thickness and the mirror-difference binding energy per nucleon; results for additional nuclei and $\Delta{\rm N^2LO_{GO}}(450)$ are shown in the Supplemental Material [87]. The neutron skin thickness computed without the Coulomb term still exhibits a linear relationship with the isospin asymmetry. However, unlike the relation shown in Fig. 4, $\Delta({\rm BE}/A)$ computed without the Coulomb term also exhibits a linear relationship with the isospin asymmetry instead of $I_{\rm C}$. This quantity entirely reflects the effects of the isospin-symmetry-breaking terms in the chiral interaction, which account for ∼1% of $\Delta({\rm BE}/A)$. These results might be useful to constrain the charge-symmetry-breaking term in Skyrme density functional theory according to Ref. [105].

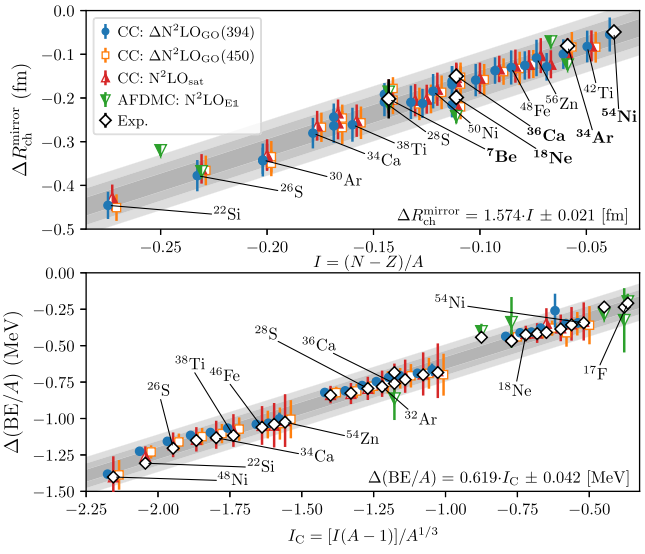


FIG. 4. Top panel: Mirror-difference charge radii plotted against the isospin asymmetry compared with experiment. The data markers are the same as those in Fig. 1. The linear regression of our data is printed in the bottom left with $1\sigma$ uncertainty, and the $1\sigma$, $2\sigma$, and $3\sigma$ confidence levels are shown as gray bands. Selected neutron-deficient nuclei are labeled. Experimental data are shown as open white diamonds, taken from Ref. [24] except for those of $^{36}$Ca [18] and $^{54}$Ni [96]. Bottom panel: Mirror-difference binding energy per nucleon $\Delta({\rm BE}/A)$ as a function of the Coulomb asymmetry. Experimental data are taken from Ref. [88].

TABLE I. Neutron skin thickness ($\Delta R_{\rm np}$) and mirror-difference binding energy per nucleon [$\Delta({\rm BE}/A)$] of select nuclei using $\Delta{\rm N^2LO_{GO}}(394)$ with and without the Coulomb term (Coul.).

| | $\Delta R_{\rm np}$ (fm) | | $\Delta({\rm BE}/A)$ (MeV) | |
|---|---|---|---|---|
| | w/ Coul. | w/o Coul. | w/ Coul. | w/o Coul. |
| $^{42}$Ca | 0.019(35) | 0.060(34) | 0.349(18) | 0.004(15) |
| $^{46}$Ca | 0.113(35) | 0.151(35) | 1.039(25) | 0.011(20) |
| $^{48}$Ca | 0.150(36) | 0.186(35) | 1.382(28) | 0.015(23) |
| $^{48}$Ti | 0.049(37) | 0.090(36) | 0.689(29) | 0.007(24) |
| $^{48}$Cr | −0.048(38) | −0.001(36) | 0.000(30) | 0.000(26) |

*Conclusions.*—We performed CC and AFDMC calculations of neutron skins of a wide range of light- and medium-mass nuclei using different interactions from chiral EFT, and found a robust linear relationship with the isospin asymmetry in agreement with the liquid-drop model. When extrapolated to heavy nuclei, this relationship is consistent with the available data. Additionally, we found a similar linear relationship between the neutron and proton radii of mirror nuclei pairs which can be used to estimate neutron radii of rare isotopes not yet accessible by experiment. Our calculations are in good agreement with available data for the difference in charge radii and binding energies of mirror nuclei. Finally, we estimated the contributions from charge-symmetry-breaking terms in the nuclear interaction which can be useful for constraining those terms in Skyrme density functionals.

We would like to thank J. Carlson, I. Tews, and R. F. Garcia Ruiz for helpful discussions. The work of S. G., S. N., and D. L. was supported by the DOE NUCLEI SciDAC Program, and by the DOE Early Career Research Program. The work of S. G. was also supported by U.S. Department of Energy, Office of Science, Office of Nuclear Physics, under Contract No. DE-AC52-06NA25396. G. H. was supported by the Office of Nuclear Physics, U.S. Department of Energy, under Grant No. DE-SC0018223 (NUCLEI SciDAC-4 collaboration) and under contract DE-AC05-00OR22725 with UT-Battelle, LLC (Oak Ridge National Laboratory). Computer time was provided by the Innovative and Novel Computational Impact on Theory and Experiment (INCITE) program. This research used resources of the Oak Ridge Leadership Computing Facility located at ORNL, which is supported by the Office of Science of the Department of Energy under Contract No. DE-AC05-00OR22725. This research also used resources provided by the Los Alamos National Laboratory Institutional Computing Program, which is supported by the U.S. Department of Energy National Nuclear Security Administration under Contract No. 89233218CNA000001.

*Present address: XCP-2, Eulerian Codes Group, Los Alamos National Laboratory, Los Alamos, New Mexico 87545, USA.

[1] B. A. Brown, Phys. Rev. Lett. **85**, 5296 (2000).
[2] C. J. Horowitz and J. Piekarewicz, Phys. Rev. Lett. **86**, 5647 (2001).
[3] C. J. Horowitz and J. Piekarewicz, Phys. Rev. C **64**, 062802(R) (2001).
[4] S. Gandolfi, J. Carlson, and S. Reddy, Phys. Rev. C **85**, 032801(R) (2012).
[5] B. P. Abbott, R. Abbott, T. D. Abbott, F. Acernese, K. Ackley, C. Adams, T. Adams, P. Addesso, R. X. Adhikari, V. B. Adya, C. Affeldt, M. Afrough, B. Agarwal, M. Agathos, K. Agatsuma *et al.* (LIGO Scientific Collaboration and Virgo Collaboration), Phys. Rev. Lett. **119**, 161101 (2017).
[6] B. P. Abbott, R. Abbott, T. D. Abbott, F. Acernese, K. Ackley, C. Adams, T. Adams, P. Addesso, R. X. Adhikari, V. B. Adya, C. Affeldt, M. Afrough, B. Agarwal, M. Agathos, K. Agatsuma *et al.*, Astrophys. J. **848**, L12 (2017).
[7] M. Al-Mamun, A. W. Steiner, J. Nättilä, J. Lange, R. O'Shaughnessy, I. Tews, S. Gandolfi, C. Heinke, and S. Han, Phys. Rev. Lett. **126**, 061101 (2021).
[8] S. Abrahamyan, Z. Ahmed, H. Albataineh, K. Aniol, D. S. Armstrong, W. Armstrong, T. Averett, B. Babineau, A. Barbieri, V. Bellini, R. Beminiwattha, J. Benesch, F. Benmokhtar, T. Bielarski, W. Boeglin *et al.* (PREX Collaboration), Phys. Rev. Lett. **108**, 112502 (2012).
[9] D. Adhikari, H. Albataineh, D. Androic, K. Aniol, D. S. Armstrong, T. Averett, C. Ayerbe Gayoso, S. Barcus, V. Bellini, R. S. Beminiwattha, J. F. Benesch, H. Bhatt, D. Bhatta Pathak, D. Bhetuwal, B. Blaikie *et al.* (PREX Collaboration), Phys. Rev. Lett. **126**, 172502 (2021).
[10] D. Adhikari, H. Albataineh, D. Androic, K. A. Aniol, D. S. Armstrong, T. Averett, C. Ayerbe Gayoso, S. K. Barcus, V. Bellini, R. S. Beminiwattha, J. F. Benesch, H. Bhatt, D. Bhatta Pathak, D. Bhetuwal, B. Blaikie *et al.* (CREX Collaboration), Phys. Rev. Lett. **129**, 042501 (2022).
[11] M. B. Tsang, J. R. Stone, F. Camera, P. Danielewicz, S. Gandolfi, K. Hebeler, C. J. Horowitz, J. Lee, W. G. Lynch, Z. Kohley, R. Lemmon, P. Möller, T. Murakami, S. Riordan, X. Roca-Maza, F. Sammarruca, A. W. Steiner, I. Vidaña, and S. J. Yennello, Phys. Rev. C **86**, 015803 (2012).
[12] G. Hagen, A. Ekström, C. Forssén, G. R. Jansen, W. Nazarewicz, T. Papenbrock, K. A. Wendt, S. Bacca, N. Barnea, B. Carlsson, C. Drischler, K. Hebeler, M. Hjorth-Jensen, M. Miorelli, G. Orlandini, A. Schwenk, and J. Simonis, Nat. Phys. **12**, 186 (2016).
[13] B. A. Brown, Phys. Rev. Lett. **119**, 122502 (2017).
[14] F. J. Fattoyev, J. Piekarewicz, and C. J. Horowitz, Phys. Rev. Lett. **120**, 172702 (2018).
[15] C. A. Bertulani and J. Valencia, Phys. Rev. C **100**, 015802 (2019).
[16] Á. Koszorús *et al.*, Nat. Phys. **17**, 439 (2021).
[17] R. F. Garcia Ruiz *et al.*, Nat. Phys. **12**, 594 (2016).
[18] A. J. Miller *et al.*, Nat. Phys. **15**, 432 (2019).
[19] S. Malbrunot-Ettenauer *et al.*, Phys. Rev. Lett. **128**, 022502 (2022).
[20] M. L. Bissell, T. Carette, K. T. Flanagan, P. Vingerhoets, J. Billowes, K. Blaum, B. Cheal, S. Fritzsche, M. Godefroid, M. Kowalska, J. Krämer, R. Neugart, G. Neyens, W. Nörtershäuser, and D. T. Yordanov, Phys. Rev. C **93**, 064318 (2016).
[21] R. P. de Groote *et al.*, Nat. Phys. **16**, 620 (2020).
[22] M. Reponen *et al.*, Nat. Commun. **12**, 4596 (2021).
[23] C. De Jager, H. De Vries, and C. De Vries, At. Data Nucl. Data Tables **14**, 479 (1974), nuclear Charge and Moment Distributions.
[24] I. Angeli and K. Marinova, At. Data Nucl. Data Tables **99**, 69 (2013).
[25] J. Piekarewicz and S. Weppner, Nucl. Phys. **A778**, 10 (2006).
[26] P.-G. Reinhard, X. Roca-Maza, and W. Nazarewicz, Phys. Rev. Lett. **129**, 232501 (2022).

[27] F. Coester, Nucl. Phys. **7**, 421 (1958).
[28] F. Coester and H. Kümmel, Nucl. Phys. **17**, 477 (1960).
[29] J. Čížek, J. Chem. Phys. **45**, 4256 (1966).
[30] J. Čížek, On the use of the cluster expansion and the technique of diagrams in calculations of correlation effects in atoms and molecules, in *Advances in Chemical Physics* (John Wiley & Sons, Inc., New York, 2007), pp. 35–89.
[31] H. Kümmel, K. H. Lührmann, and J. G. Zabolitzky, Phys. Rep. **36**, 1 (1978).
[32] R. J. Bartlett and M. Musiał, Rev. Mod. Phys. **79**, 291 (2007).
[33] G. Hagen, T. Papenbrock, M. Hjorth-Jensen, and D. J. Dean, Rep. Prog. Phys. **77**, 096302 (2014).
[34] K. E. Schmidt and S. Fantoni, Phys. Lett. B **446**, 99 (1999).
[35] J. Carlson, S. Gandolfi, F. Pederiva, S. C. Pieper, R. Schiavilla, K. E. Schmidt, and R. B. Wiringa, Rev. Mod. Phys. **87**, 1067 (2015).
[36] D. Lonardoni, S. Gandolfi, J. E. Lynn, C. Petrie, J. Carlson, K. E. Schmidt, and A. Schwenk, Phys. Rev. C **97**, 044318 (2018).
[37] E. Epelbaum, H.-W. Hammer, and U.-G. Meißner, Rev. Mod. Phys. **81**, 1773 (2009).
[38] R. Machleidt and D. Entem, Phys. Rep. **503**, 1 (2011).
[39] K. Hebeler, S. K. Bogner, R. J. Furnstahl, A. Nogga, and A. Schwenk, Phys. Rev. C **83**, 031301(R) (2011).
[40] A. Ekström, G. Baardsen, C. Forssén, G. Hagen, M. Hjorth-Jensen, G. R. Jansen, R. Machleidt, W. Nazarewicz, T. Papenbrock, J. Sarich, and S. M. Wild, Phys. Rev. Lett. **110**, 192502 (2013).
[41] D. R. Entem, N. Kaiser, R. Machleidt, and Y. Nosyk, Phys. Rev. C **91**, 014002 (2015).
[42] E. Epelbaum, H. Krebs, and U.-G. Meißner, Phys. Rev. Lett. **115**, 122301 (2015).
[43] T. Hüther, K. Vobig, K. Hebeler, R. Machleidt, and R. Roth, Phys. Lett. B **808**, 135651 (2020).
[44] V. Somà, P. Navrátil, F. Raimondi, C. Barbieri, and T. Duguet, Phys. Rev. C **101**, 014318 (2020).
[45] A. Ekström, B. D. Carlsson, K. A. Wendt, C. Forssén, M. H. Jensen, R. Machleidt, and S. M. Wild, J. Phys. G **42**, 034003 (2015).
[46] C. G. Payne, S. Bacca, G. Hagen, W. G. Jiang, and T. Papenbrock, Phys. Rev. C **100**, 061304(R) (2019).
[47] S. Bagchi *et al.*, Phys. Rev. Lett. **124**, 222504 (2020).
[48] W. G. Jiang, A. Ekström, C. Forssén, G. Hagen, G. R. Jansen, and T. Papenbrock, Phys. Rev. C **102**, 054301 (2020).
[49] A. Tichai, J. Müller, K. Vobig, and R. Roth, Phys. Rev. C **99**, 034321 (2019).
[50] S. J. Novario, G. Hagen, G. R. Jansen, and T. Papenbrock, Phys. Rev. C **102**, 051303(R) (2020).
[51] G. Hagen, T. Papenbrock, D. J. Dean, A. Schwenk, A. Nogga, M. Włoch, and P. Piecuch, Phys. Rev. C **76**, 034302 (2007).
[52] R. Roth, S. Binder, K. Vobig, A. Calci, J. Langhammer, and P. Navrátil, Phys. Rev. Lett. **109**, 052501 (2012).
[53] A. Gezerlis, I. Tews, E. Epelbaum, S. Gandolfi, K. Hebeler, A. Nogga, and A. Schwenk, Phys. Rev. Lett. **111**, 032501 (2013).
[54] A. Gezerlis, I. Tews, E. Epelbaum, M. Freunek, S. Gandolfi, K. Hebeler, A. Nogga, and A. Schwenk, Phys. Rev. C **90**, 054323 (2014).
[55] J. E. Lynn, I. Tews, J. Carlson, S. Gandolfi, A. Gezerlis, K. E. Schmidt, and A. Schwenk, Phys. Rev. Lett. **116**, 062501 (2016).
[56] J. E. Lynn, J. Carlson, E. Epelbaum, S. Gandolfi, A. Gezerlis, and A. Schwenk, Phys. Rev. Lett. **113**, 192501 (2014).
[57] J. E. Lynn, I. Tews, J. Carlson, S. Gandolfi, A. Gezerlis, K. E. Schmidt, and A. Schwenk, Phys. Rev. C **96**, 054007 (2017).
[58] D. Lonardoni, J. Carlson, S. Gandolfi, J. E. Lynn, K. E. Schmidt, A. Schwenk, and X. B. Wang, Phys. Rev. Lett. **120**, 122502 (2018).
[59] D. Lonardoni, S. Gandolfi, X. B. Wang, and J. Carlson, Phys. Rev. C **98**, 014322 (2018).
[60] J. E. Lynn, D. Lonardoni, J. Carlson, J.-W. Chen, W. Detmold, S. Gandolfi, and A. Schwenk, J. Phys. G **47**, 045109 (2020).
[61] S. H. Lim, J. Carlson, C. Loizides, D. Lonardoni, J. E. Lynn, J. L. Nagle, J. D. Orjuela Koop, and J. Ouellette, Phys. Rev. C **99**, 044904 (2019).
[62] R. Cruz-Torres, S. Li, F. Hauenstein, A. Schmidt, D. Nguyen, D. Abrams, H. Albataineh, S. Alsalmi, D. Androic, K. Aniol, W. Armstrong, J. Arrington, H. Atac, T. Averett, C. Ayerbe Gayoso *et al.*, Phys. Lett. B **797**, 134890 (2019).
[63] R. Cruz-Torres, D. Lonardoni, R. Weiss, M. Piarulli, N. Barnea, D. W. Higinbotham, E. Piasetzky, A. Schmidt, L. B. Weinstein, R. B. Wiringa, and O. Hen, Nat. Phys. **17**, 306 (2021).
[64] P. W. Zhao and S. Gandolfi, Phys. Rev. C **94**, 041302(R) (2016).
[65] P. Klos, J. E. Lynn, I. Tews, S. Gandolfi, A. Gezerlis, H.-W. Hammer, M. Hoferichter, and A. Schwenk, Phys. Rev. C **94**, 054005 (2016).
[66] S. Gandolfi, H.-W. Hammer, P. Klos, J. E. Lynn, and A. Schwenk, Phys. Rev. Lett. **118**, 232501 (2017).
[67] I. Tews, S. Gandolfi, A. Gezerlis, and A. Schwenk, Phys. Rev. C **93**, 024305 (2016).
[68] M. Buraczynski and A. Gezerlis, Phys. Rev. Lett. **116**, 152501 (2016).
[69] M. Buraczynski and A. Gezerlis, Phys. Rev. C **95**, 044309 (2017).
[70] L. Riz, S. Gandolfi, and F. Pederiva, J. Phys. G **47**, 045106 (2020).
[71] I. Tews, J. Carlson, S. Gandolfi, and S. Reddy, Astrophys. J. **860**, 149 (2018).
[72] I. Tews, J. Margueron, and S. Reddy, Phys. Rev. C **98**, 045804 (2018).
[73] S. Gandolfi, J. Carlson, A. Roggero, J. E. Lynn, and S. Reddy, Phys. Lett. B **785**, 232 (2018).
[74] I. Tews, J. Margueron, and S. Reddy, Eur. Phys. J. A **55**, 97 (2019).
[75] D. Lonardoni, I. Tews, S. Gandolfi, and J. Carlson, Phys. Rev. Res. **2**, 022033(R) (2020).
[76] L. Riz, F. Pederiva, D. Lonardoni, and S. Gandolfi, Particles **3**, 706 (2020).
[77] H. Hergert, Front. Phys. **8**, 379 (2020).
[78] S. Gandolfi, D. Lonardoni, A. Lovato, and M. Piarulli, Front. Phys. **8**, 117 (2020).
[79] W. D. Myers and W. Swiatecki, Ann. Phys. (N.Y.) **55**, 395 (1969).

[80] W. Myers and W. Swiatecki, Ann. Phys. (N.Y.) **84**, 186 (1974).
[81] W. D. Myers, *Droplet Model of Atomic Nuclei* (IFI/Plenum Data Company, New York, USA, 1977).
[82] W. Myers and W. Swiatecki, Nucl. Phys. **A336**, 267 (1980).
[83] C. J. Pethick and D. G. Ravenhall, Nucl. Phys. **A606**, 173 (1996).
[84] S. Kaufmann *et al.*, Phys. Rev. Lett. **124**, 132502 (2020).
[85] M. Miorelli, S. Bacca, G. Hagen, and T. Papenbrock, Phys. Rev. C **98**, 014324 (2018).
[86] G. Hagen, S. J. Novario, Z. H. Sun, T. Papenbrock, G. R. Jansen, J. G. Lietz, T. Duguet, and A. Tichai, Phys. Rev. C **105**, 064311 (2022).
[87] See Supplemental Material at http://link.aps.org/supplemental/10.1103/PhysRevLett.130.032501 for additional results and derivations of LDM corrections, which includes Refs. [24,32,79–82,88,89].
[88] M. Wang, G. Audi, F. G. Kondev, W. Huang, S. Naimi, and X. Xu, Chin. Phys. C **41**, 030003 (2017).
[89] G. Hagen, T. Papenbrock, D. J. Dean, M. Hjorth-Jensen, and B. V. Asokan, Phys. Rev. C **80**, 021306(R) (2009).
[90] A. Trzcińska, J. Jastrzębski, P. Lubiński, F. J. Hartmann, R. Schmidt, T. von Egidy, and B. Kłos, Phys. Rev. Lett. **87**, 082501 (2001).
[91] J. Jastrzębski, A. Trzcińska, P. Lubiński, B. Kłos, F. J. Hartmann, T. von Egidy, and S. Wycech, Int. J. Mod. Phys. E **13**, 343 (2004).
[92] V. Lapoux, V. Somà, C. Barbieri, H. Hergert, J. D. Holt, and S. R. Stroberg, Phys. Rev. Lett. **117**, 052501 (2016).
[93] J. Zenihiro, H. Sakaguchi, S. Terashima, T. Uesaka, G. Hagen, M. Itoh, T. Murakami, Y. Nakatsugawa, T. Ohnishi, H. Sagawa, H. Takeda, M. Uchida, H. P. Yoshida, S. Yoshida, and M. Yosoi, arXiv:1810.11796.
[94] M. Warda, X. Viñas, X. Roca-Maza, and M. Centelles, Phys. Rev. C **80**, 024316 (2009).
[95] B. Hu, W. Jiang, T. Miyagi, Z. Sun, A. Ekström, C. Forssén, G. Hagen, J. D. Holt, T. Papenbrock, S. R. Stroberg, and I. Vernon, Nat. Phys. **18**, 1196 (2022).
[96] S. V. Pineda, K. König, D. M. Rossi, B. A. Brown, A. Incorvati, J. Lantis, K. Minamisono, W. Nörtershäuser, J. Piekarewicz, R. Powel, and F. Sommer, Phys. Rev. Lett. **127**, 182503 (2021).
[97] J. D. Holt, J. Menéndez, and A. Schwenk, Phys. Rev. Lett. **110**, 022502 (2013).
[98] T. D. Morris, J. Simonis, S. R. Stroberg, C. Stumpf, G. Hagen, J. D. Holt, G. R. Jansen, T. Papenbrock, R. Roth, and A. Schwenk, Phys. Rev. Lett. **120**, 152503 (2018).
[99] N. Michel, J. G. Li, F. R. Xu, and W. Zuo, Phys. Rev. C **100**, 064303 (2019).
[100] J. S. Randhawa *et al.*, Phys. Rev. C **99**, 021301 (2019).
[101] S. R. Stroberg, J. D. Holt, A. Schwenk, and J. Simonis, Phys. Rev. Lett. **126**, 022501 (2021).
[102] R. Pohl, A. Antognini, F. Nez, F. D. Amaro, F. Biraben, J. M. Cardoso, D. S. Covita, A. Dax, S. Dhawan, L. M. Fernandes, A. Giesen, T. Graf, T. W. Hänsch, P. Indelicato, L. Julien *et al.*, Nature (London) **466**, 213 (2010).
[103] W. Xiong, A. Gasparian, H. Gao, D. Dutta, M. Khandaker, N. Liyanage, E. Pasyuk, C. Peng, X. Bai, L. Ye, K. Gnanvo, C. Gu, M. Levillain, X. Yan, D. W. Higinbotham *et al.*, Nature (London) **575**, 147 (2019).
[104] A. A. Filin, V. Baru, E. Epelbaum, H. Krebs, D. Möller, and P. Reinert, Phys. Rev. Lett. **124**, 082501 (2020).
[105] T. Naito, G. Colò, H. Liang, X. Roca-Maza, and H. Sagawa, Phys. Rev. C **105**, L021304 (2022).